Introduction

This paper is concerned with the computation of stable and unstable manifolds of unstable periodic orbits using the method of Lagrangian descriptors (LDs) (Jiménez Madrid and Mancho 2009; Craven and Hernandez 2016, 2015; Craven, Junginger, and Hernandez 2017; Junginger et al. 2016, 2017, 2016; Feldmaier et al. 2017, 2017; Patra and Keshavamurthy 2018). We illustrate this method by applying it to understand the phase space structure governing the roaming reaction mechanism (Suits 2008; Bowman and Shepler 2011; Bowman and Suits 2011; Bowman 2014; Mauguière et al. 2017) in a setting where the system of interest is subjected to a nonholonomic constraint that enforces constant kinetic energy (Dettmann and Morriss 1996; Morriss and Dettmann 1998; Litniewski 1993; Morishita 2003). First we give some background on this problem.

The roaming mechanism for chemical reactions was discovered in efforts to explain certain experimental data describing the photodissociation of formaldehyde (Zee, Foltz, and Moore 1993; Townsend et al. 2004; Bowman 2006). Roaming provides a route to molecular dissociation products H_2 and CO that does not involve passage through a conventional transition state. After excitation of the formaldehyde molecule (H_2CO) by a laser pulse, a single CH bond begins to stretch. Rather than proceed directly to dissociation, one hydrogen atom rotates around the molecular fragment in a flat region of the potential energy surface; at a later stage this roaming hydrogen atom encounters the bound hydrogen atom and undergoes an abstraction reaction. The resulting H_2 molecule then separates from the CO fragment. This reaction is then said to occur by the roaming mechanism.

Since the pioneering formaldehyde studies roaming has been observed to occur in a number of chemical reactions, which are discussed in a number of review articles (Suits 2008; Bowman and Shepler 2011; Bowman and Suits 2011; Bowman 2014; Mauguière et al. 2017).

We note that essentially all of these roaming reactions have been studied at constant total energy.

Chesnavich developed an empirical model (Chesnavich 1986) for the ion-molecule reaction $CH_4^+ \rightleftharpoons CH_3^+ + H$ that contains the essential features of the roaming mechanism. A detailed derivation of this model can be found in (Ezra and Wiggins 2019). Chesnavich's model describes the situation where a hydrogen atom separates from a rigid CH_3^+ core and, instead of dissociating, roams in a region of nearly constant potential only to return to the core. While Chesnavich's model does not accurately describe the intramolecular abstraction and subsequent dissociation, it has nevertheless provided significant insight into the roaming process, see, for example, (Mauguière, Collins, Ezra, Farantos, et al. 2014a, 2014b; V. Krajňák and Waalkens 2018; V. Krajňák and Wiggins 2018).

The goal of this article is to extend our previous study of the analogous roaming reaction mechanisms at constant kinetic energy (Krajňák, Ezra, and Wiggins

2019). We do this by applying a Hamiltonian isokinetic thermostat (Dettmann and Morriss 1996; Morriss and Dettmann 1998; Litniewski 1993; Morishita 2003) to Chesnavich's model. Use of the isokinetic thermostat means that we are effectively investigating roaming at constant temperature. A detailed study of Chesnavich's model subjected to the Hamiltonian isokinetic thermostat is given in (Krajňák, Ezra, and Wiggins 2019). In that work it was found that certain of the periodic orbits that govern the roaming dynamics are highly unstable: their Lyapunov exponents are $\sim 10^{21}$. In such a situation detection of the periodic orbits, as well as the computation of their stable and unstable manifolds, becomes problematic using traditional approaches.

In this paper we show that the method of Lagrangian descriptors (Jiménez Madrid and Mancho 2009; Craven and Hernandez 2016, 2015; Craven, Junginger, and Hernandez 2017; Junginger et al. 2016, 2017, 2016; Feldmaier et al. 2017, 2017; Patra and Keshavamurthy 2018) can be used to compute stable and unstable manifolds of such highly unstable periodic orbits. We applying this approach to Chesnavich's model subjected to a Hamiltonian isokinetic thermostat and show that the method of Lagrangian descriptors reveals the dynamical origin of the roaming mechanism in this setting.

This paper is outlined as follows: In Sec. 2 we introduce Chesnavich's Hamiltonian model for ion-molecule reaction and discuss the dynamical mechanism underlying roaming in terms of families of unstable periodic orbits and their associated invariant manifolds. In Sec. 3 we discuss the Hamiltonian formulation of the isokinetic thermostat for Chesnavich's CH_4^+ model. In Sec. 4 we introduce the method of Lagrangian descriptors and use prior knowledge of periodic orbits to construct a Lagrangian descriptor for detecting stable and unstable invariant manifolds. We then apply the method to Chesnavich's model subjected to a Hamiltonian isokinetic thermostat to reveal the roaming mechanism in this system. Sec. 5 concludes.

Chesnavich's Model and Roaming

Chesnavich's Model Hamiltonian

The CH_4^+ model due to Chesnavich is a 2 degree of freedom Hamiltonian system comprised of a rigid CH_3^+ molecule (core) and a mobile H atom (Chesnavich 1986). The system Hamiltonian is (Ezra and Wiggins 2019)

$$H(r, \theta, p_r, p_\theta) = \frac{1}{2}\frac{p_r^2}{\mu} + \frac{1}{2}p_\theta^2 \left(\frac{1}{\mu r^2} + \frac{1}{I_{CH_3}} \right) + U(r, \theta), \qquad (1)$$

where (r, θ, ϕ) are polar coordinates describing the position of the H-atom in a body-fixed frame attached to the CH_3^+ core (the coordinate ϕ is ignorable in this model). The reduced mass of the system is given by the expression

$\mu = \frac{m_{CH_3} m_H}{m_{CH_3} + m_H}$, where $m_H = 1.007825$ u and $m_{CH_3} = 3m_H + 12.0$ u, and the moment of inertia of the rigid body CH_3^+ has the value $I_{CH_3} = 2.373409$ uÅ^2.

The potential energy function $U(r, \theta)$ is made up of a radial long range potential energy term U_{CH} and a short range potential U_{coup} that models the short range anisotropy of the rigid CH_3^+ core:

$$U(r, \theta) = U_{CH}(r) + U_{coup}(r, \theta). \tag{2}$$

The topography of the potential energy surface is characterised by two deep wells that correspond to the bound CH_4^+, two areas of high potential and a flat area to the outside of these features as shown in Fig. [fig:pot].
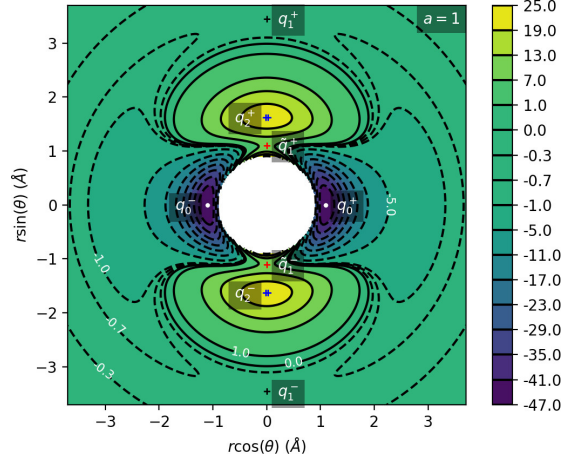

Figure 1: Contour plot of Chesnavich's potential energy surface U for $a = 1$. Dashed lines correspond to $U < 0$, solid lines correspond to $U \geq 0$. Contours correspond to values of potential shown on the colorbar to the right, with some values indicated in the plot. This figure is from (V. Krajňák and Wiggins 2018).

The long range potential has the form:

$$U_{CH}(r) = \frac{D_e}{c_1 - 6} \left(2(3 - c_2)e^{c_1(1-x)} - (4c_2 - c_1 c_2 + c_1) x^{-6} - (c_1 - 6)c_2 x^{-4} \right), \tag{3}$$

where $x = \frac{r}{r_e}$ and we take the parameter values as in the original work (Chesnavich 1986). The short range hindered rotor potential U_{coup} has the form:

$$U_{coup}(r, \theta) = \frac{U_e e^{-a(r-r_e)^2}}{2}(1 - \cos 2\theta), \tag{4}$$

where U_e is the equilibrium barrier height. The distance at which the transition occurs from rotation to vibration is determined by the parameter a (in Å^{-2}).

3

Various values of a have been considered in previous works. In particular, $a = 1$ (Chesnavich 1986; Mauguière, Collins, Ezra, Farantos, et al. 2014b, 2014a; V. Krajňák and Waalkens 2018), $a = 4$ (Chesnavich 1986; Mauguière, Collins, Ezra, Farantos, et al. 2014b) and a range of values $0.7 \leq a \leq 8$. (V. Krajňák and Wiggins 2018)

The CH_3^+ core is a symmetric top in Chesnavich's model. Although the range of the coordinate θ is $0 \leq \theta \leq \pi$, in the planar (zero overall angular momentum) version of the model the range of θ is extended to $0 \leq \theta \leq 2\pi$, and the potential has a four-fold symmetry:

$$U(r, \theta) = U(r, -\theta) = U(r, \pi - \theta) = U(r, \pi + \theta). \tag{5}$$

The potential admits four pairs of equilibrium points pairwise related by symmetry [eq:sym], as listed in Tab. [table:equil] and shown in Fig. [fig:pot].

Table 1: Equilibrium points of the potential $U(r, \theta)$.

Energy (kcal mol^{-1})	r (Å)	θ (radians)	Significance	Label
-47	1.1	0	potential well	q_0^+
-0.63	3.45	$\pi/2$	isomerisation saddle	q_1^+
8	1.1	$\pi/2$	isomerisation saddle	$\widetilde{q}_1^+$
22.27	1.63	$\pi/2$	local maximum	q_2^+

Roaming in Chesnavich's Model {#sec:roamingChes}

In this work a Lagrangian descriptor approach to computing invariant manifolds is applied to an analysis of the roaming mechanism for chemical reaction dynamics. In the context of the CH_4^+ model of Chesnavich this means we want to uncover the phase space mechanism whereby the hydrogen atom separates from the CH_3^+ core and later returns to the core before dissociating. We now review the dynamical definition of roaming that was introduced in (Mauguière, Collins, Ezra, Farantos, et al. 2014b), which is based on periodic orbits as the phase space structures governing the dynamics of roaming.

In the relevant energy interval, $0 \leq E \leq 5$, there are three families of periodic orbits that organize the roaming dynamics in phase space (Mauguière, Collins, Ezra, Farantos, et al. 2014a). These periodic orbits are pairwise related by symmetry [eq:sym], as shown in Fig. [fig:orbitse5]. We will refer to these families as the inner (Γ^i), middle (Γ^a) and outer (Γ^o) periodic orbits. We refer to a continuum of periodic orbits parametrised by energy as a family of periodic orbits. We highlight the fact that none of the orbits is directly related to a saddle point on the potential energy surface.

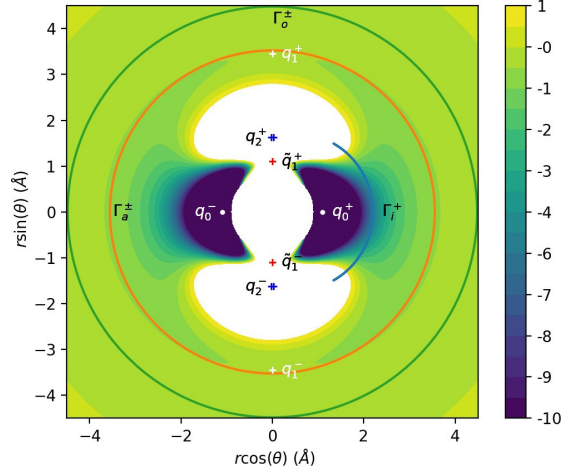The significance of these periodic orbits for the roaming dynamics is as follows:

Figure 2: Configuration space projections of the inner (Γ^i), middle (Γ^a) and outer (Γ^o) periodic orbits for $E = 5$. This figure is from (Krajňák, Ezra, and Wiggins 2019).

- Γ^i: Delimits the potential wells that correspond to CH_4^+ isomers. The orbits oscillate about the axes $\theta = 0$ and $\theta = \pi$.

- Γ^a: Two rotational orbits with opposite orientation - one clockwise, one counter-clockwise - that are crucial for defining roaming.

- Γ^o: Centrifugal barrier delimiting the region of dissociated states. Two rotational orbits with opposite orientation - one clockwise, one counter-clockwise.

It was shown in (V. Krajňák and Waalkens 2018) that roaming does not occur for $E \geq 2.5$. In the energy interval $0 < E < 2.5$, all of the above-mentioned periodic orbits are unstable. We use these periodic orbits to define dividing surfaces. Denote by DS^i, DS^a and DS^o the set of all points $(r, \theta, p_r, p_\theta)$ on the energy surface $H(r, \theta, p_r, p_\theta) = E$, whose configuration space projections (r, θ) coincide with the configuration space projections of Γ^i, Γ^a and Γ^o respectively. Due to the instability of the orbits, the resulting dividing surfaces satisfy the non-recrossing properties.

A roaming trajectory is then defined as a trajectory that crosses DS^a an odd number of times between leaving the potential well and dissociating. An isomerising trajectory leaves the potential well, crosses DS^a an even number of times and returns to either of the potential wells. A nonreactive trajectory originates in dissociated states and returns there after an even number of crossings of DS^a.

As explained in (V. Krajňák and Waalkens 2018), DS^i consists of two spheres because Γ^i is comprised of self-retracing (brake) orbits, while the rotational orbits Γ^a and Γ^o imply that DS^a and DS^o are tori (Mauguière et al. 2016).

Each sphere can be divided using the corresponding periodic orbit into two hemispheres and each torus can be divided using both corresponding periodic orbits into two annuli (Mauguière et al. 2016). All hemispheres and annuli are surfaces of unidirectional flux. This implies that all trajectories leaving the potential well cross the same (outward) hemisphere of DS^i, while all trajectories entering the potential well cross the other (inward) hemisphere of DS^i.

Roaming can be described as a transport problem in phase space. Every trajectory leaving the well must cross the outward hemisphere of DS^i and every trajectory that dissociates must cross the outward annulus of DS^o. Dissociation of CH_4^+ is therefore equivalent to the transport of trajectories from the outward hemisphere of DS^i to the outward annulus of DS^o. Roaming involves crossing the inward annulus of DS^a, since between two crossings of the outward annulus trajectories must cross the inward annulus and vice versa.

Transport of trajectories in the neighbourhood of an unstable periodic orbit (or NHIM in general) is governed by invariant manifolds of the orbit (Wiggins et al. 2001; Uzer et al. 2002; Waalkens, Schubert, and Wiggins 2008; Wiggins 2016). It was shown (V. Krajňák and Waalkens 2018; V. Krajňák and Wiggins 2018) that the roaming phenomenon involves a heteroclinic intersection of the invariant manifolds of Γ^i and Γ^o. The condition $H(r, \theta = 0, p_r > 0, p_\theta = 0)$ defines an invariant subsystem that consists of precisely one dissociating trajectory for every fixed $E > 0$. Therefore if the invariant manifolds of Γ^i and Γ^o do not intersect, the former are contained in the interior of the latter and each trajectory leaving the potential well dissociates directly. An intersection assures that some trajectories leaving the well do not dissociate directly but return to DS^a as illustrated in Fig. [fig:DSa]. This is the phase space mechanism for roaming and isomerisation in the Hamiltonian case.

The Hamiltonian Isokinetic Thermostat for the Chesnavich Model {#sec: HIK}

Here we apply the Hamiltonian isokinetic thermostat to the Chesnavich model. Details of the theory behind the Hamiltonian isokinetic thermostate model in this context can be found in (Krajňák, Ezra, and Wiggins 2019). Here we just give the relevant equations with a brief description.

The isokinetic Hamiltonian $\mathcal{K}$ for Chesnavich's model is

$$\mathcal{K}(r, \pi_r, \theta, \pi_\theta) = \frac{1}{2}e^U\left(\frac{\pi_r^2}{\mu} + \pi_\theta^2\left(\frac{1}{\mu r^2} + \frac{1}{I_{CH_3}}\right)\right) - \frac{1}{2}e^{-U}, \qquad (6)$$

where $U = U(r, \theta)$ is Chesnavich's potential energy and

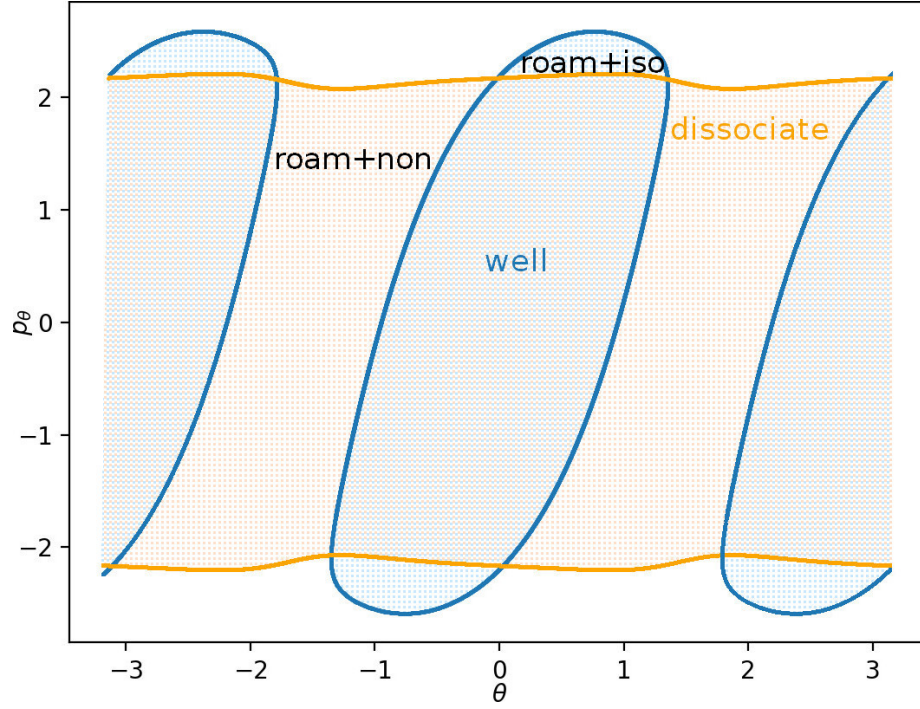$$\pi_r = e^{-U}p_r, \quad \pi_\theta = e^{-U}p_\theta. \qquad (7)$$

Figure 3: Intersection of invariant manifolds of Γ^i (blue) and Γ^o (orange) with the outward annulus of DS^a for $E = 1$. Trajectories that just left the potential well are shown in blue, immediately dissociating trajectories in orange. Roaming and isomerising trajectories in the blue area just left the well and do not dissociate immediately, while roaming and dissociating trajectories in the orange are dissociate immediately but did not just leave the potential wells. This figure is from (Krajňák, Ezra, and Wiggins 2019).

The level set $\mathcal{K} = 0$ corresponds to the surface of constant kinetic energy

$$\frac{1}{2}\frac{p_r^2}{\mu} + \frac{1}{2}p_\theta^2\left(\frac{1}{\mu r^2} + \frac{1}{I_{CH_3}}\right) = \frac{1}{2}, \tag{8}$$

in system [eq:chesHam]. We fix the kinetic energy at $\frac{1}{2}$, because according to (Krajňák, Ezra, and Wiggins 2019) the dynamics generated by [eq:chesKHam] is equivalent regardless of the value of kinetic energy (up to a time rescaling). This statement remains true for other systems provided that the kinetic energy is a quadratic form in the momenta.

The equations of motion in the isokinetic system in terms of variables $(r, \pi_r, \theta, \pi_\theta)$ are given in (Krajňák, Ezra, and Wiggins 2019). To achieve greater numerical precision, it is preferable to integrate the equations of motion in the $(r, p_r, \theta, p_\theta)$ coordinates instead of the $(r, \pi_r, \theta, \pi_\theta)$ (Krajňák, Ezra, and Wiggins 2019):

$$\begin{aligned}
\dot{r} &= \frac{p_r}{\mu}, \\
\dot{p}_r &= p_r\left(\frac{\partial U}{\partial r}\dot{r} + \frac{\partial U}{\partial \theta}\dot{\theta}\right) + \frac{1}{\mu r^3}p_\theta^2 - \frac{\partial U}{\partial r}, \\
\dot{\theta} &= p_\theta\left(\frac{1}{\mu r^2} + \frac{1}{I_{CH_3}}\right), \\
\dot{p}_\theta &= p_\theta\left(\frac{\partial U}{\partial r}\dot{r} + \frac{\partial U}{\partial \theta}\dot{\theta}\right) - \frac{\partial U}{\partial \theta},
\end{aligned} \tag{9}$$

where we used the isokinetic constraint [eq:constantT] equivalent to $\mathcal{K} = 0$.

The potential $-\frac{1}{2}e^{-U}$ has the same critical points and characteristics as U, but the wells are considerably deeper and have steeper walls. In contrast to the microcanonical case, the isokinetic model only possesses two periodic orbits with period 2π and due to constant nonzero kinetic energy does not admit self-retracing orbits (also referred to as brake orbits) such as Γ^i introduced in Section 2.2. One of the periodic orbits delimits the potential wells, see Fig. [fig:disI]; we therefore refer to it as the inner orbit.

The outer orbit, beyond which trajectories do not return and corresponds to the dissociated state of the molecule, is associated with a centrifugal barrier. It is nearly rotationally symmetric and in double precision has a constant radius $r = 13.4309241401910709$.

Its existence can be proven using a similar argument as in the original system (V. Krajňák and Waalkens 2018): suppose r is sufficiently large so that U is effectively independent of θ. Denote r_{po} the solution of

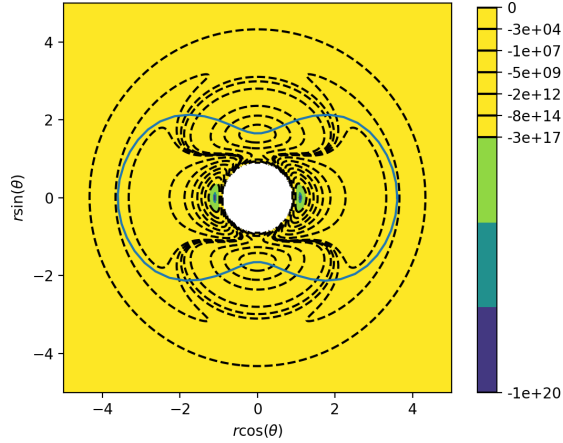$$\frac{1}{\mu r_{po}^3}p_\theta^2 - \frac{\partial U}{\partial r} = 0.$$

Figure 4: Inner periodic orbit on the potential energy surface $-\frac{1}{2}e^{-U}$. This figure is from (Krajňák, Ezra, and Wiggins 2019).

Then the equations [eq:chesKHameqreduced] admit a rotationally symmetric periodic orbit with $\dot{\theta} = const$, provided

$$\dot{r} = 0,$$
$$\dot{p}_r = 0.$$

This is satisfied by the initial condition $r = r_{po}$, $p_r = 0$ and p_θ given implicitly by $\mathcal{K} = 0$ for any θ. The existence of r_{po} is guaranteed for the potential U and any other potential with leading order term $-cr^{-(2+\varepsilon)}$ for large r, with $c > 0$ and $\varepsilon > 0$.

Both these orbits are unstable, with the largest eigenvalue of the inner orbit under the return map being of the order 10^{21}. This large instability poses a serious challenge to calculation of its invariant manifolds that guide trajectories in phase space. We therefore employ the method of Lagrangian descriptors to find these invariant manifolds.

Lagrangian descriptors and invariant manifolds

Introduction to Lagrangian descriptors

Lagrangian descriptors are a very successful trajectory diagnostic for revealing phase space structures in dynamical systems. The method was originally developed for analyzing Lagrangian transport phenomena in fluid dynamics (Jiménez Madrid and Mancho 2009). but the utility and applicability of the method has recently been recognized in chemistry (Craven and Hernandez 2016, 2015; Craven,

Junginger, and Hernandez 2017; Junginger et al. 2016, 2017, 2016; Feldmaier et al. 2017, 2017; Patra and Keshavamurthy 2018). The method is simple to implement computationally, the interpretation in terms of trajectory behaviour is clear, and it provides a 'high resolution' method for exploring high-dimensional phase space with low-dimensional slices (Demian and Wiggins 2017; Naik and Wiggins 2019; Naik, García-Garrido, and Wiggins 2019; García-Garrido, Naik, and Wiggins 2019). It applies to Hamiltonian and non-Hamiltonian systems (Lopesino et al. 2017) and to systems with arbitrary, even stochastic, time-dependence (Balibrea-Iniesta et al. 2016) Moreover, Lagrangian descriptors can be applied directly to data sets, without the need of an explicit dynamical system (Mendoza, Mancho, and Wiggins 2014).

Lagrangian descriptors minimised by invariant manifolds

Complementary to existing applications of Lagrangian descriptors as an exploratory method, we use Lagrangian descriptors to find invariant manifolds in a system where some invariant structures have already been identified. In the present case we use the parametrisation of a periodic orbit to construct a Lagrangian descriptor that will be locally minimised by its invariant manifolds.

For a Hamiltonian system with 2 degrees of freedom and (q_1, p_1, q_2, p_2) as phase space coordinates, a 1 dimensional periodic orbit Γ can be viewed as an intersection of three hypersurfaces: the surface of constant energy it lives on and two other distinct hypersurfaces that parametrise Γ, $f_1(q_1, p_1, q_2, p_2) = 0$ and $f_2(q_1, p_1, q_2, p_2) = 0$. For a system with zero total angular momentum, these equations can correspond to the configuration space projection and parametrisation of one of the momenta.

The integral

$$\int_0^\infty |\dot{f}_i(q_1, p_1, q_2, p_2)| dt, \tag{10}$$

then vanishes along the periodic orbit for $i = 1, 2$.

As $t \to \infty$, $f_1, f_2 \to 0$ along the periodic orbit stable invariant manifolds. Consequently of all points on the energy surface, [eq:LDinfty] is locally minimised by those that lie on the stable invariant manifold of Γ. Necessarily this statement remains true for the finite time integral

$$\int_0^\tau |\dot{f}_i(q, p)| dt, \qquad i = 1, 2,$$

provided $\tau > 0$ is large enough. We can use the same argument for the unstable

invariant manifold and the Lagrangian descriptor

$$\int\limits_{-\tau}^{0} |\dot{f}_i(q,p)|dt, \qquad i = 1, 2.$$

Depending on the strength of instability of Γ, small values of τ may suffice to find an approximate location of the invariant manifolds and to establish whether or not they intersect, which is a crucial characteristic for the presence of roaming.

Roaming in the Isokinetic Chesnavich Model

In (Krajňák, Ezra, and Wiggins 2019), we established the presence of roaming and classified dynamical behaviour using escape time analysis and Lagrangian descriptors. Classes of qualitatively different dynamical behaviour are separated by invariant manifolds, since these guide trajectories across phase space bottlenecks.

Due to the large instability of the inner orbit, it was not previously possible to compute its invariant manifolds to create an analogue of Fig. [fig:DSa]. The Lagrangian descriptors defined in Sec. 4.2 uncover trajectories in the proximity of invariant manifolds and we thereby avoid having to compute invariant manifolds at all.

As for the microcanonical version of Chesnavich's model, we are interested in the following manifolds:

- the unstable manifold of the inner orbit W_i^u, which guides trajectories out of the wells into the interaction region between DS^i and DS^o,

- the stable manifold of the outer orbit W_o^s, which guides trajectories out of the interaction region towards dissociation.

We now construct the Lagrangian descriptors described in Sec. 4.2. The inner periodic orbit is parametrised by

$$f_1(r, \theta) = r - \bar{r}(\theta) = 0,$$

where

$$\bar{r}(\theta) = c_0 + c_1 \cos(2\theta) + c_2 \cos(4\theta) + c_3 \cos(6\theta) + c_4 \cos(8\theta) + c_5 \cos(10\theta),$$

with constants

$$c_0 = 2.78147867, \ c_1 = 0.98235111, \ c_2 = -0.17161848,$$
$$c_3 = -0.00486657, \ c_4 = 0.01628185, \ c_5 = -0.00393858,$$

and

$$f_2(\theta, p_r) = p_r - \bar{p}_r(\theta) = 0,$$

11

where $\bar{p}_r(\theta)$ is a function defined for $\theta \in (-\frac{\pi}{2}, \frac{\pi}{2}]$ and periodically extended to $\theta \in \mathbb{R}$, given by

$$\bar{p}_r(\theta) = d_0\theta + d_1\theta^3 + d_2\theta^5 + d_3\theta^7 + d_4\theta^9 + d_5\theta^{11},$$

with constants

$$d_0 = -1.06278495, \ d_1 = -0.42089795, \ d_2 = 1.38849679,$$
$$d_3 = -1.11654771, \ d_4 = 0.40789372, \ d_5 = -0.05122644.$$

Note that the periodic orbit need only be parametrised for a single value of $\mathcal{K}$, $\mathcal{K} = 0$.

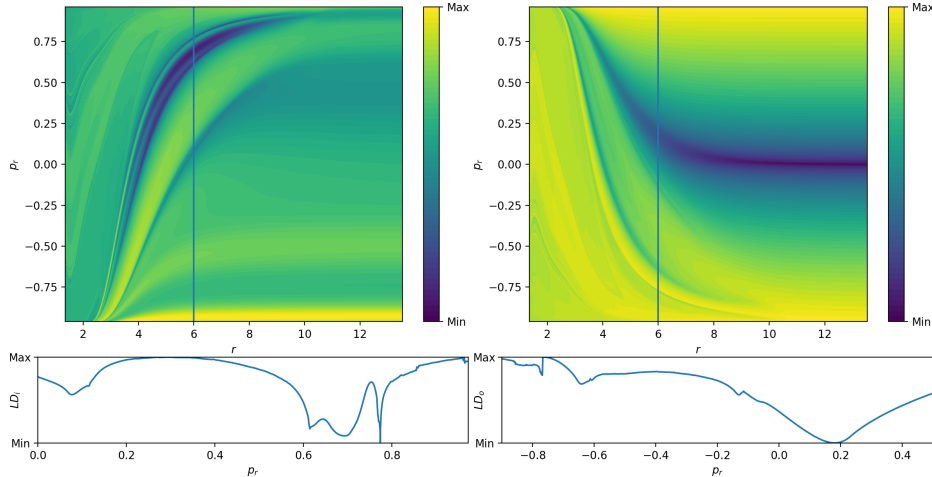To identify W_i^u, we use the Lagrangian descriptor

$$LD_i = \int\limits_{-\tau}^{0} |\dot{r} - \bar{r}'(\theta)\dot{\theta}|dt. \tag{11}$$

Note that we obtain identical results using

$$\int\limits_{-\tau}^{0} |\dot{p}_r - \bar{p}_r'(\theta)\dot{\theta}|dt.$$

We approximate the outer periodic orbit by a constant radius $r = 13.4309241401910709$ and its stable invariant manifold W_o^s locally minimises

$$LD_o = \int\limits_{0}^{\tau} |\dot{r}|dt. \tag{12}$$
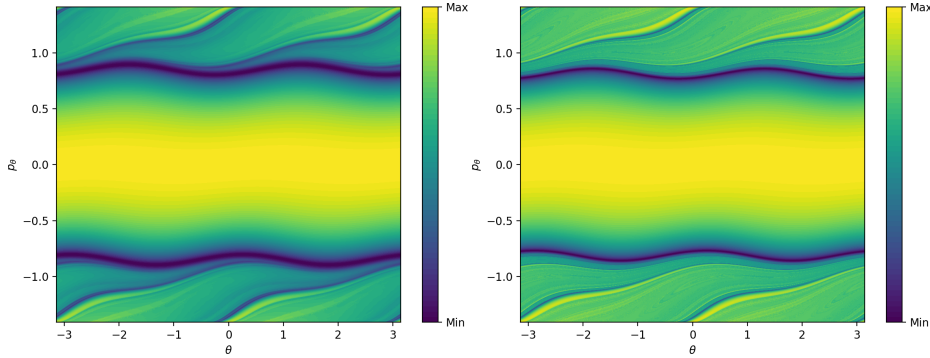

[fig:manifs__th0]

In (Krajňák, Ezra, and Wiggins 2019), we found that singularities in the escape time plot matched significant changes in Lagrangian descriptor plots. Both these features indicated the presence of invariant manifolds. In Fig. [fig:manifs_th0] we show LD_i [eq:LDi] and LD_o [eq:LDo] on the surface $\theta = 0$, $\dot{\theta} > 0$, where the latter is similar to the plots in (Krajňák, Ezra, and Wiggins 2019) and the former shows similar features reflected about $p_r = 0$ due to the opposite time direction in the definition of LD_i. Both plots show LD values on a uniform 400×400 grid. A higher density improves accuracy but does not yield additional qualitative information. The accompanying sections for $r = 6$ illustrate the nature of the local minima.

The presence of roaming is only possible if W_i^u and W_o^s intersect (V. Krajňák and Waalkens 2018). Fig. [fig:manifs_th0] provides direct evidence of the intersection - the two panels show W_i^u and W_o^s using different Lagrangian descriptors on the same surface of section. These manifolds necessarily intersect.
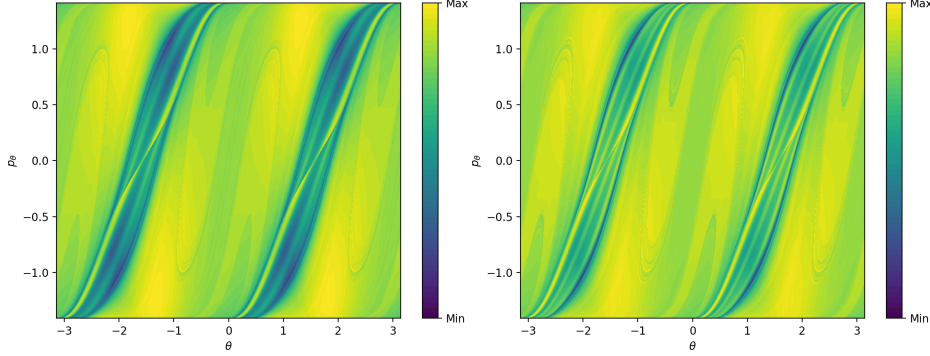
[fig:manifsI_r36]

Further information on the geometry of the intersection of W_i^u and W_o^s can be seen using a surface of section analogous to the outward annulus of DS^a used in the Hamiltonian case.

[fig:manifsO_r36]

Due to the absence of other 2π-periodic orbits, one cannot expect to easily obtain

13

a surface of section that is transversal to the flow. For simplicity, we use a surface of section defined by the condition $r = 3.6$, $\dot{r} > 0$. Figures [fig:manifsI_r36] and [fig:manifsO_r36] show LD_i [eq:LDi] and LD_o [eq:LDo] on this surface. Areas of low values of LD_i and LD_o correspond to trajectories that are asymptotic to the respective periodic orbits. Note that the structures are well defined visually for times that are of the same order of magnitude as the periodic orbits themselves - periods of the inner and outer orbits are 11.84 and 9.61 respectively.

Similarly to the microcanonical case, the toriodal cylinder W_o^s intersects $r = 3.6$, $\dot{r} > 0$ transversally in two circles, one with $p_\theta > 0$, one with $p_\theta < 0$.

W_i^u has the same geometry as W_o^s, but it does not intersect the surface of section transversally. This can be seen by the manifold attaining maximal p_θ permitted by kinetic energy $\frac{1}{2}$, when p_r vanishes and $\dot{r} > 0$ is violated. As a result, instead of two circles, the two unstable invariant manifolds intersect the surface of section in four S-shapes. The initial condition $\theta = p_\theta = 0$ leads to radial dissociation, and it is surrounded by trajectories that originate in the well. This area is bounded by two of the S-shapes - the S-shape passing closest to $\theta = 1$, $p_\theta = 0$ corresponds to the inner periodic orbit with $p_\theta > 0$. The S-shape closest to $\theta = -1$, $p_\theta = 0$ corresponds to the inner periodic orbit with $p_\theta < 0$. The other S-shapes are related by symmetry.

Fig. [fig:intersection] shows superposed manifolds approximated from LD_i ($\tau = 6$) and LD_o ($\tau = 20$) values. Minima of LD_o for fixed values of θ reveal W_o^s immediately.

Due to the high instability of the inner orbit, locating W_i^u using minima of LD_i requires a very dense sampling with a correspondingly high computational cost. (Note how narrow the interval for finding the minimum on the profile of LD_i on $\theta = 0$, $r = 6$ in Fig. [fig:manifs_th0] is.) Instead we can take advantage of the steepnes of the gradient near the invariant manifold and consider maxima of $\Delta_\theta LD_i$ on a 400×400 grid for fixed p_θ values. This way we recover the four S-shapes due to W_i^u. Applying a cutoff at high values of LD_i before calculating $\Delta_\theta LD_i$ delivers a cleaner image; in Fig. [fig:intersection] we used a cutoff at $\frac{1}{2}(\max_{LD_i} + \min_{LD_i})$.

Aside from W_i^u, Fig. [fig:intersection] shows traces of two nearly linear segments near W_i^u pointing towards the points $\theta = \frac{\pi}{2}$, $p_\theta = 0$ and $\theta = \frac{3\pi}{2}$, $p_\theta = 0$ on the surface of section. These are initial conditions of trajectories asymptotic to the manifolds $\theta = \frac{\pi}{2}$, $p_\theta = 0$, $p_r > 0$ and $\theta = \frac{3\pi}{2}$, $p_\theta = 0$, $p_r > 0$. (Due to conservation of kinetic energy, these manifolds are distinct from $\theta = \frac{\pi}{2}$, $p_\theta = 0$, $p_r < 0$ and $\theta = \frac{3\pi}{2}$, $p_\theta = 0$, $p_r < 0$.)

Having identified W_i^u and W_o^s, we can observe that these invariant manifolds guide trajectories in the same way as in the microcanonical model. Fig. [fig:intersection] is analogous to Fig. [fig:DSa]. The area between the two circles of W_o^s is crossed by trajectories that are led by W_o^s to dissociation. The area containing $\theta = p_\theta = 0$ between two of the S-shapes of W_i^u is crossed by trajectories that originate in the well.
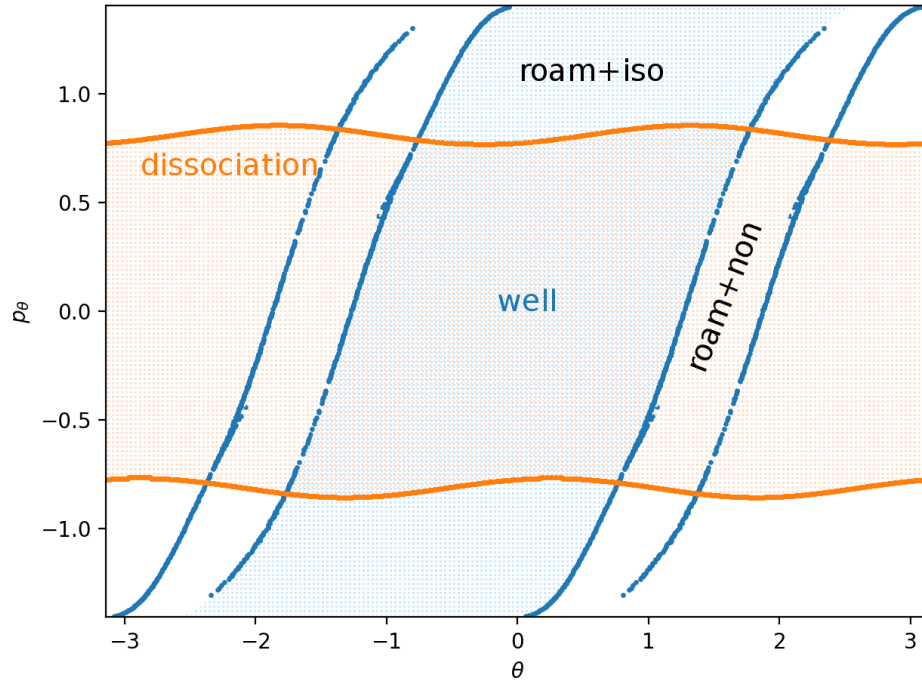
14

Figure 5: Approximations of invariant manifolds on $r = 3.6$, $\dot{r} > 0$ extracted from LD_i for $\tau = 6$ shown in Fig. [fig:manifsI_r36] and LD_o for $\tau = 20$ shown in Fig [fig:manifsO_r36] that separate different classes of dynamics. For details see text.

Clearly the intersection of these two areas contains directly dissociating initial conditions. The complement between two of the S-shapes contains isomerising and roaming trajectories; in fact it is here the trajectories cross the surface of section for the first time after leaving the well. Similarly we observe a band between the two circles of W_o^s which is crossed by trajectories that do not just leave the well. These may be roaming trajectories that originate in the well and recross the surface or nonreactive trajectories that never enter the well at all. This band marks the last crossing of the surface by these trajectories before dissociation. The remaining area corresponds to trajectories that stay in the interaction region before entering one of the wells or dissociating.

It is important to note that all classes of dynamics are separated by an intricate fractal structure made up of invariant manifolds, as shown in (Krajňák, Ezra, and Wiggins 2019). The structure becomes visible when integrating any Lagrangian descriptor over a long time interval, see the details of Fig. [fig:manifsI_r36] and [fig:manifsO_r36].

Conclusions and Outlook

We have shown how to compute stable and unstable invariant manifolds for which traditional methods fail due to high instability of the corresponding periodic orbit. For this purpose we propose the construction of a Lagrangian descriptor defined using an explicit parametrisation of the periodic orbit. The method is simple and easy to implement because it does not require calculating eigendirections of the orbit. Additional advantages follow from lower demands on accuracy.

Invariant manifolds obtained this way enabled us to compare roaming in Chesnavich's CH_4^+ model and the isokinetic version of Chesnavich's CH_4^+ model subject to a Hamiltonian isokinetic theromostat. We conclude that regardless of detailed differences in phase space structures, the invariant structures responsibles for roaming bear remarkable similarities despite the nonholonomic constraint of constant kinetic energy.

Balibrea-Iniesta, F., C. Lopesino, S. Wiggins, and A. M. Mancho. 2016. "Lagrangian Descriptors for Stochastic Differential Equations: A Tool for Revealing the Phase Portrait of Stochastic Dynamical Systems." *Int. J. Bifurcation Chaos* 26 (13). World Scientific: 1630036. https://doi.org/10.1142/S0218127416300366.

Bowman, J. M. 2006. "Skirting the Transition State, a New Paradigm in Reaction Rate Theory." *Proc. Nat. Acad. Sci.* 103 (44): 16061–2. https://doi.org/10.1073/pnas.0607810103.

———. 2014. "Roaming." *Mol. Phys.* 112 (19): 2516–28. https://doi.org/10.1080/00268976.2014.897395.

Bowman, J. M., and B. C. Shepler. 2011. "Roaming Radicals." *Annu. Rev. Phys. Chem.* 62: 531–53. https://doi.org/10.1146/annurev-physchem-032210-103518.

Bowman, J. M., and A. G. Suits. 2011. "Roaming reaction: The third way." *Phys. Today* 64 (11). AIP: 33. https://doi.org/10.1063/PT.3.1330.

Chesnavich, W. J. 1986. "Multiple Transition States in Unimolecular Reactions." *J. Chem. Phys.* 84 (5): 2615–9. https://doi.org/10.1063/1.450331.

Craven, G. T., and R. Hernandez. 2015. "Lagrangian Descriptors of Thermalized Transition States on Time-Varying Energy Surfaces." *Phys. Rev. Lett.* 115 (14). APS: 148301. https://doi.org/10.1103/PhysRevLett.115.148301.

———. 2016. "Deconstructing Field-Induced Ketene Isomerization Through Lagrangian Descriptors." *Phys. Chem. Chem. Phys.* 18 (5). Royal Society of Chemistry: 4008–18. https://doi.org/10.1039/C5CP06624G.

Craven, G. T., A. Junginger, and R. Hernandez. 2017. "Lagrangian Descriptors of Driven Chemical Reaction Manifolds." *Phys. Rev. E* 96 (2). APS: 022222. https://doi.org/10.1103/PhysRevE.96.022222.

Demian, A. S., and S. Wiggins. 2017. "Detection of Periodic Orbits in Hamiltonian Systems Using Lagrangian Descriptors." *Int. J. Bifurcation Chaos* 27 (14). World Scientific: 1750225. https://doi.org/10.1142/S021812741750225X.

Dettmann, C. P., and G. P. Morriss. 1996. "Hamiltonian formulation of the Gaussian isokinetic thermostat." *Phys. Rev. E* 54: 2495–2500. https://doi.org/10.1103/PhysRevE.54.2495.

Ezra, G. S., and S. Wiggins. 2019. "The Chesnavich Model for Ion-Molecule Reactions: A Rigid Body Coupled to a Particle." *Int. J. Bifurcation Chaos* 29 (02). World Scientific: 1950025. https://doi.org/10.1142/S0218127419500251.

Feldmaier, M., A. Junginger, J. Main, G. Wunner, and R. Hernandez. 2017. "Obtaining Time-Dependent Multi-Dimensional Dividing Surfaces Using Lagrangian Descriptors." *Chem. Phys. Lett.* 687. Elsevier: 194–99. https://doi.org/10.1016/j.cplett.2017.09.008.

García-Garrido, V. J., S. Naik, and S. Wiggins. 2019. "Tilting and Squeezing: Phase Space Geometry of Hamiltonian Saddle-Node Bifurcation and Its Influence on Chemical Reaction Dynamics." *arXiv Preprint arXiv:1907.03322.*

Jiménez Madrid, J. A., and A. M. Mancho. 2009. "Distinguished Trajectories in Time Dependent Vector Fields." *Chaos* 19: 013111. https://doi.org/10.1063/1.3056050.

Junginger, A., G. T. Craven, T. Bartsch, F. Revuelta, F. Borondo, R. M. Benito, and R. Hernandez. 2016. "Transition State Geometry of Driven Chemical Reactions on Time-Dependent Double-Well Potentials." *Phys. Chem. Chem. Phys.* 18 (44). Royal Society of Chemistry: 30270–81. https://doi.org/10.1039/C6CP02519F.

Junginger, A., L. Duvenbeck, M. Feldmaier, J. Main, G. Wunner, and R. Hernandez. 2017. "Chemical Dynamics Between Wells Across a Time-Dependent

Barrier: Self-Similarity in the Lagrangian Descriptor and Reactive Basins." *J. Chem. Phys.* 147 (6): 064101. https://doi.org/10.1063/1.4997379.

Krajňák, V, G. S. Ezra, and S. Wiggins. 2019. "Roaming at Constant Kinetic Energy: Chesnavich's Model and the Hamiltonian Isokinetic Thermostat." *Submitted to Regul. Chaotic Dyn.*

Krajňák, V., and H. Waalkens. 2018. "The Phase Space Geometry Underlying Roaming Reaction Dynamics." *J. Math. Chem.* Springer, 1–38. https://doi.org/10.1007/s10910-018-0895-4.

Krajňák, V., and S. Wiggins. 2018. "Influence of Mass and Potential Energy Surface Geometry on Roaming in Chesnavich's Ch 4+ Model." *J. Chem. Phys.* 149 (9). AIP Publishing: 094109. https://doi.org/10.1063/1.5044532.

Litniewski, M. 1993. "Molecular dynamics method for simulating constant temperature-volume and constant temperature-pressure systems." *J. Phys. Chem.* 97: 3842–8. https://doi.org/10.1021/j100117a035.

Lopesino, C., F. Balibrea-Iniesta, V. J. García-Garrido, S. Wiggins, and A. M. Mancho. 2017. "A Theoretical Framework for Lagrangian Descriptors." *Int. J. Bifurcation Chaos* 27 (01): 1730001. https://doi.org/10.1142/S0218127417300014.

Mauguière, F. A. L., P. Collins, G. S. Ezra, S. C Farantos, and S. Wiggins. 2014a. "Multiple Transition States and Roaming in Ion–Molecule Reactions: A Phase Space Perspective." *Chem. Phys. Lett.* 592. Elsevier: 282–87. https://doi.org/10.1016/j.cplett.2013.12.051.

Mauguière, F. A. L., P. Collins, G. S. Ezra, S. C. Farantos, and S. Wiggins. 2014b. "Roaming Dynamics in Ion-Molecule Reactions: Phase Space Reaction Pathways and Geometrical Interpretation." *J. Chem. Phys.* 140 (13). AIP Publishing: 134112. https://doi.org/10.1063/1.4870060.

Mauguière, F. A. L., P. Collins, Z. C. Kramer, B. K. Carpenter, G. S. Ezra, S. C. Farantos, and S. Wiggins. 2016. "Phase space barriers and dividing surfaces in the absence of critical points of the potential energy: Application to roaming in ozone." *J. Chem. Phys.* 144: 054107. https://doi.org/10.1063/1.4940798.

———. 2017. "Roaming: A Phase Space Perspective." *Annu. Rev. Phys. Chem.* 68 (1). Annual Reviews 4139 El Camino Way, PO Box 10139, Palo Alto, California 94303-0139, USA. https://doi.org/10.1146/annurev-physchem-052516-050613.

Mendoza, C., A.M. Mancho, and S. Wiggins. 2014. "Lagrangian Descriptors and the Assessment of the Predictive Capacity of Oceanic Data Sets." *Nonlin. Processes Geophys.* 21 (3). Copernicus GmbH: 677–89. https://doi.org/10.5194/npg-21-677-2014.

Morishita, T. 2003. "Generalized coupling to a heat bath: Extension of the Gaussian isokinetic dynamics and effect of time scaling." *J. Chem. Phys.* 119:

7075–82. https://doi.org/10.1063/1.1605731.

Morriss, G. P., and C. P. Dettmann. 1998. "Thermostats: Analysis and application." *Chaos* 8: 321–36. https://doi.org/10.1063/1.166314.

Naik, S., V. J. García-Garrido, and S. Wiggins. 2019. "Finding Nhim: Identifying High Dimensional Phase Space Structures in Reaction Dynamics Using Lagrangian Descriptors." *arXiv Preprint arXiv:1903.10264.*

Naik, S., and S. Wiggins. 2019. "Finding Normally Hyperbolic Invariant Manifolds in Two and Three Degrees of Freedom with Hénon-Heiles-Type Potential." *Phys. Rev. E* 100 (2). American Physical Society: 022204. https://doi.org/10.1103/PhysRevE.100.022204.

Patra, S., and S. Keshavamurthy. 2018. "Detecting Reactive Islands Using Lagrangian Descriptors and the Relevance to Transition Path Sampling." *Phys. Chem. Chem. Phys.* 20 (7). Royal Society of Chemistry: 4970–81. https://doi.org/10.1039/C7CP05912D.

Suits, A. G. 2008. "Roaming Atoms and Radicals: A New Mechanism in Molecular Dissociation." *Acc. Chem. Res.* 41 (7): 873–81. https://doi.org/10.1021/ar8000734.

Townsend, D., S.A. Lahankar, S. K. Lee, S. D. Chambreau, A. G. Suits, X. Zhang, J. Rheinecker, L. B. Harding, and J. M. Bowman. 2004. "The roaming atom: Straying from the reaction path in formaldehyde decomposition." *Science* 306 (5699). American Association for the Advancement of Science: 1158–61. https://doi.org/10.1126/science.1104386.

Uzer, T., C. Jaffé, J. Palacián, P. Yanguas, and S. Wiggins. 2002. "The Geometry of Reaction Dynamics." *Nonlinearity* 15 (4). IOP Publishing: 957. https://doi.org/10.1088/0951-7715/15/4/301.

Waalkens, H., R. Schubert, and S. Wiggins. 2008. "Wigner's Dynamical Transition State Theory in Phase Space: Classical and Quantum." *Nonlinearity* 21 (1): R1–R118. https://doi.org/10.1088/0951-7715/21/1/R01.

Wiggins, S. 2016. "The Role of Normally Hyperbolic Invariant Manifolds (Nhims) in the Context of the Phase Space Setting for Chemical Reaction Dynamics." *Regul. Chaotic Dyn.* 21 (6). Springer: 621–38. https://doi.org/10.1134/S1560354716060034.

Wiggins, S., L. Wiesenfeld, C. Jaffe, and T. Uzer. 2001. "Impenetrable Barriers in Phase-Space." *Phys. Rev. Lett.* 86(24): 5478–81. https://doi.org/10.1103/PhysRevLett.86.5478.

Zee, R. D. van, M. F. Foltz, and C. B. Moore. 1993. "Evidence for a second molecular channel in the fragmentation of formaldehyde." *J. Chem. Phys.* 99 (3). AIP: 1664–73. https://doi.org/10.1063/1.465335.